Face-Centered Cubic and Hexagonal Closed-Packed Nanocrystal Superlattices of Gold Nanoparticles Prepared by Different Methods[†]

Savka I. Stoeva,[‡] B. L. V. Prasad,[‡] Sitharaman Uma,[‡] Peter K. Stoimenov,[‡] Vladimir Zaikovski,[||] Christopher M. Sorensen,[§] and Kenneth J. Klabunde*,[‡]

Department of Chemistry and Department of Physics, Kansas State University, Manhattan, Kansas 66506, and Boreskov Institute of Catalysis, Novosibirsk 630090, Russia

Dodecanethiol-stabilized gold nanoparticles with similar average size organize into different superlattice structures depending upon the method of preparation of the nanocrystals. Particles synthesized by the inverse micelle technique preferentially assemble into face-centered cubic (fcc) structures with long-range translational and orientational ordering. Gold nanoparticles obtained by the solvated metal atom dispersion (SMAD) method behave like "hard" spheres and predominantly organize into hexagonal close-packed (hcp) nanocrystal superlattices with long-range translational ordering. Different packing behavior results from differences in nanoparticle core morphologies induced by the synthetic method; fcc ordering is preferred by single crystalline nanoparticles, while hcp is preferred by polycrystalline nanoparticles. A combination of optical microscopy, transmission electron microscopy (TEM and HRTEM), selected area electron diffraction (SAED), atomic force microscopy (AFM), and X-ray diffraction (XRD) were used to characterize both the dispersed nanoparticles and the nanocrystal superlattices.

Introduction

Two- and three-dimensional ordered arrays of nanoparticles, known as nanocrystal superlattices (NCSLs), comprise one of the most fascinating classes of nanomaterials. Close-packed nanocrystal assemblies are ideal systems for studying novel chemical and physical phenomena arising from the collective interaction of the constituting units. The tremendous interest in nanocrystal superlattices is also driven by their already established or envisioned applications in various fields, where optical, electronic transport, and magnetic properties change with nanocrystal organization.[1−8] Development of synthetic methods that lead to high-quality nanoparticles has enabled the formation of long-range-ordered nanocrystal superlattices composed of metal,[7,9−20] semiconductor,[8,21−23] and magnetic nanocrystals.[1,24−27]

Utilization of nanocrystal superlattices in practice inevitably requires the ability to control not only the parameters (size and shape) of the separate building units, but also the three-dimensional (3D) crystal structure of the nanoparticle assembly. Several research groups have addressed this issue. Most of the studies concentrated on self-organization of gold and silver nanoparticles stabilized by variable chain-length alkane-thiols[9,10,15,16,28−30] primarily because these two systems have proven to be ideal in the respect that they are relatively easy to handle and have a strong propensity toward superlattice formation. The morphology of the nanocrystalline core may, indeed, be important in affecting nanoparticle organization. In fact, Whetten and co-workers have reported both face-centered cubic (fcc) and hexagonal close-packed (hcp) long-range structures, which apparently were the result of different core structures of
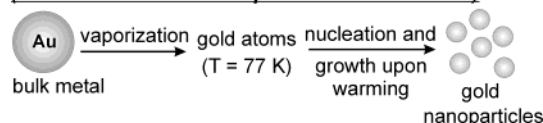

Figure 1. Different synthetic routes used for preparation of gold nanoparticles.

the silver nanoparticles.[15,16] These examples suggest that faceting of the nanoparticle core may dictate the bundling and inter-digitation of the ligand molecules, causing the particles to arrange into different superlattice structures. In this regard, the role of stabilizing molecules in nanoparticle arrangement was theoretically studied by Luedke and Landman.[31] Molecular dynamic simulations predicted that alkanethiols adsorbed on Au nanocrystallites organized into molecular bundles of preferred orientation. The room-temperature equilibrium structure of a superlattice composed of dodecanethiol-stabilized faceted Au nanoparticles was predicted to be tetragonally distorted fcc.[31]

It is generally believed that the ratio of metal core size to ligand chain length is the main parameter that governs the nanocrystal superlattice's packing.[28,32−34] An intriguing question, however, is whether particles with similar size and stabilized by the same ligand can adopt different superlattice structures.

In the present paper, we report that dodecanethiol-stabilized Au nanoparticles with similar size self-assemble into fcc or hcp nanocrystal superlattices depending upon the method of their preparation. We have utilized two completely different synthetic routes (Figure 1). High-quality Au nanoparticles are reproducibly

prepared by both methods, and they behave as molecular crystals in the respect that they can be dissolved, precipitated, and redispersed without change in properties. The first method is based on a reduction process carried out in an inverse micelle system.[14] Gold nanoparticles obtained by the inverse micelle method have an average diameter of 4.7 nm and organize in fcc nanocrystal superlattices with orientational ordering between nanocrystals. The second synthetic route involves vaporization of a metal under vacuum and co-deposition of the atoms with the vapors of a solvent on the walls of a reactor cooled to liquid nitrogen temperature (77 K). Nucleation and growth of the nanoparticles take place during the warmup stage. This procedure is known as the solvated metal atom dispersion (SMAD) method. Gold nanoparticles synthesized by the SMAD technique have an average diameter of 4.5 nm [13] and self-assemble preferentially in long-range-ordered hcp superlattices. Thus, control over nanocrystal packing can be exerted by applying different synthetic methods for their preparation. A combination of optical microscopy, electron microscopy (TEM and HRTEM), selected area electron diffraction (SAED), atomic force microscopy (AFM), and X-ray diffraction (XRD) were used to characterize both the dispersed nanoparticles and the nanocrystal superlattices.

Experimental Section

(a) Nanoparticle Preparation.

Inverse Micelle Method. A detailed description of the synthetic procedure is provided in ref 14. Briefly, 0.034 g of $AuCl_3$ (99.99%+, Aldrich) was dissolved in 10 mL of 2.2×10^{-2} M solution of didodecyldimethylammonium bromide (DDAB, Fluka) in toluene (Fisher). Reduction of the gold salt was achieved by addition of 40 μL of 9.6 M aqueous solution of $NaBH_4$ (Aldrich) while the solution was vigorously stirred. Ultrahigh purity water (18 MΩ, Millipore) was used throughout the whole experiment. Dodecanethiol (200 μL, Aldrich) was added to 2.5 mL of the as-prepared gold colloid. This was followed by nanoparticle precipitation with 7.5 mL of ethanol (Fisher) in order to purify the system from any byproducts. The precipitate was dried under dynamic vacuum and redispersed in 2.5 mL of toluene and 200 μL of dodecanethiol. The colloid was then subjected to a reflux ("digestive ripening") for 90 min under an argon atmosphere.[14] This procedure led to the formation of high-quality nanoparticles stabilized by dodecanethiol in toluene medium with an average diameter of 4.7 nm.

SMAD Method. The SMAD technique allows synthesis of large amounts of colloidal solutions and obviates the need for any purification procedures. Reference 13 provides a detailed description of the Au nanoparticle preparation by the SMAD procedure. The process was carried out under dynamic vacuum (4×10^{-3} Torr) in a stationary reactor[35] submerged in liquid nitrogen. Dodecanethiol (8 mL) and toluene (40 mL) were frozen at the bottom of the reactor. Elemental Au (0.2–0.4 g) was then evaporated and co-deposited with acetone vapors (100 mL) on the walls of the vessel. After the process was complete, the liquid nitrogen Dewar was removed and the deep red Au–acetone matrix was allowed to warm. Upon melting, the Au–acetone matrix mixed with toluene and dodecanethiol and the color of the colloidal solution became deep brown. Agitation was commenced for ~45 min. The Au–acetone–toluene–thiol solution was siphoned into a Schlenk tube, and acetone was evaporated under vacuum together with some of the toluene. The Au–toluene–thiol colloid was diluted to 80 mL. The colloid was then refluxed for 90 min under argon atmosphere
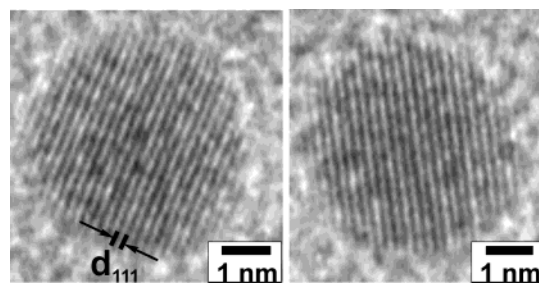

Figure 2. HRTEM images of single crystalline Au nanoparticles prepared by the inverse micelle method.

("digestive ripening"). The final colloidal solution contains high-quality Au nanoparticles stabilized by dodecanethiol with an average diameter of 4.5 nm.

(b) Nanocrystal Superlattice Formation.

Au colloidal solutions obtained by inverse micelle and SMAD methods have a strong tendency toward superlattice formation due to the uniformity in size and shape of the nanoparticles present in both systems. Nanocrystal superlattices were formed by a deposition of Au colloidal solution on a support at ambient conditions. Samples for TEM were prepared by placing a 3 μL drop of the colloidal solution onto a carbon-coated Formvar copper grid. The grids were allowed to dry in a dust-free area for several hours. In some cases, anticapillary tweezers were used in order to slow the drying process and to obviate any capillary forces. Specimens for AFM and XRD were prepared by depositing larger amounts of colloidal solution (10 μL for AFM and 50 μL for XRD) on carbon-coated or hydrophobic glass slides (modified by octyltrimethoxysilane to achieve better contact with the toluene solution). The glass slides were left undisturbed for 2–3 weeks covered in a Petri dish to ensure slow nanocrystal formation. Studies with carbon-coated supports were conducted in order to have a direct comparison with TEM results without being concerned about effects of the support.

(c) Structural Analysis.

Optical Microscopy. Optical imaging of nanocrystal superlattices deposited as thin films on a glass substrate was performed on an Axioplan 2, Carl Zeiss.

Electron Microscopy. Low-resolution TEM was performed with a Philips CM 100 operating at 100 kV. High-resolution transmission electron microscopy (HRTEM) imaging was done with a JEM-2010 (JEOL, Japan) with 1.4 Å lattice resolution and 200 kV accelerating voltage. Selected area electron diffraction (SAED), computer-simulated fast Fourier transformed (FFT) images, and Fourier filtration were used for in-depth structure analysis.

Atomic Force Microscopy. Samples were imaged on a Nanoscope IIIa (Digital instruments) in tapping mode using Olympus OTESPA 125 μm tips with typical resonance frequency of 300 kHz. Scan angle 0° and scan rate 0.2–0.5 Hz are typical scan parameters.

X-ray Diffraction. Powder X-ray diffraction patterns were recorded using a Scintag X-ray diffractometer with Cu Kα radiation. The patterns were recorded in the range 3–50° (2θ) with a step size of 0.01°.

Results and Discussion

Two levels of organization are present in nanocrystal superlattices: (i) atomic arrangement in the nanoparticles that determines their morphology; (ii) particle assembly in a superlattice structure assisted by the stabilizing molecules tethered to the nanoparticle surface. Elucidation of the structure and
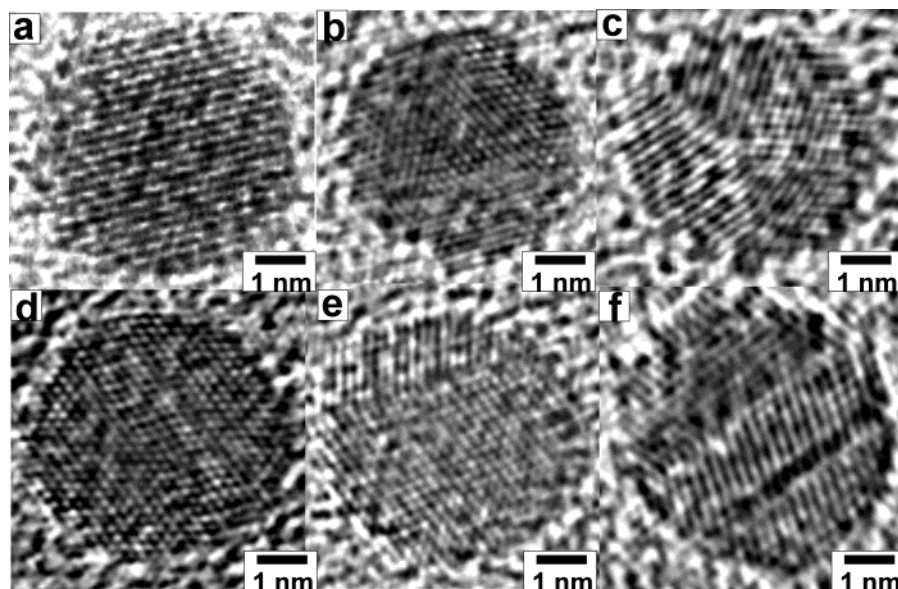
fcc and hcp Superlattices of Au Nanoparticles

J. Phys. Chem. B, Vol. 107, No. 30, 2003 **7443**

Figure 3. Fourier filtered HRTEM images of different Au nanocrystal core morphologies prepared by the SMAD method: (a) single crystal; (b) icosahedral type; (c) multiple packing defects along (111) planes; (d)−(f) particles with parallel twinning boundaries.

morphology of the building units is important in understanding the structure of the nanocrystal superlattices.

Structure of Nanoparticles Prepared by the Inverse Micelle and SMAD Methods.

HRTEM was utilized as a powerful technique for imaging the structure of nanoparticles obtained by the inverse micelle and SMAD methods. It was found that the majority of particles prepared by the reduction procedure and subsequent digestive ripening were predominantly faceted single crystals. Figure 2 exemplifies the perfect atomic arrangement in the particles where (111) atomic planes from the gold fcc lattice are clearly visible. Conversely, Au nanoparticles synthesized by the SMAD procedure and subsequent digestive ripening have a variety of structures. Figure 3 provides an overview of the different nanocrystal core morphologies present in the SMAD samples. Defect-free Au nanoparticles (Figure 3a) are rarely observed in the SMAD colloids. The majority of the gold cores have planar defects such as twinning boundaries (Figure 3d−f) and stacking faults. Multiply twinned particles such as icosahedral type (to be more precise pentagonal bipyramidal) are often observed (Figure 3b,c). Such morphologies are frequently found in noble metal particles where the bulk atomic arrangement is fcc;[28,36−39] note that normal bulk gold is fcc. The overall analysis of nanocrystal morphologies shows that the SMAD colloids are predominantly comprised of highly defective spherical particles. As we shall discuss later, this has a direct effect on the type of ordering in superlattice structures.

The differences in the nanocrystal core morphologies of the Au particles synthesized by the inverse micelle and SMAD methods can be explained by the different nature of the two synthetic techniques. Nucleation and growth in the reduction process take place under more controlled fashion compared to the SMAD case. In the vaporization method, particles nucleate and grow in a more chaotic manner during the warm stage. The presence of multiple twinning most probably results from residual stresses accumulated during the cluster growth. Though both colloids were subjected to a digestive ripening, it is unlikely that this surface process[13,14] can transform the core structures of the particles. We should take into account, however, that in the case of the inverse micelle system some residual DDAB surfactant might be present during the ripening process. It may
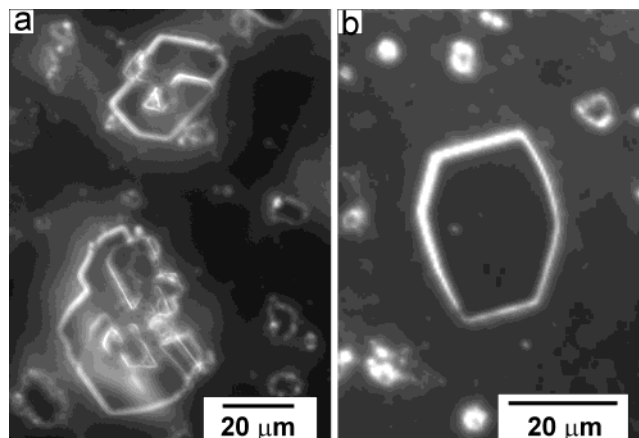

Figure 4. Dark-field optical micrographs of 3D Au colloidal crystals grown on a carbon-coated glass substrate.

influence faceting of the gold cores by preferentially adsorbing on selected planes of the particles, allowing the growth of other facets.[40] It should be pointed out that both synthetic schemes produce Au nanoparticles with uniform size and a strong affinity toward self-organization.

Gold Nanocrystal Superlattice Structures.

Nanocrystal Superlattices of Au Nanoparticles Prepared by the Inverse Micelle Method.

Dodecanethiol-stabilized Au nanocrystals synthesized by the inverse micelle method self-assemble into long-range-ordered superlattices when deposited on a support. Figure 4 represents dark-field optical micrographs of three-dimensional gold colloidal crystals grown on a carbon-coated glass slide. Formation of faceted crystals with well-defined shapes is observed, indicative of reversible crystal growth.[15] Terraces and steps are seen in the crystals shown in Figure 4a. Most probably, organization of the Au nanoparticles followed the classical model of adatom addition to a growing surface.[41] Murray and co-workers[3,8] have observed by high-resolution scanning electron microscopy a similar fashion of CdSe nanocrystal organization.

TEM of NCSLs deposited on carbon-coated grids (Figure 5) completely corroborates the optical microscopy results. In Figure 5a,b are low-magnification images of Au nanocrystal superlat-
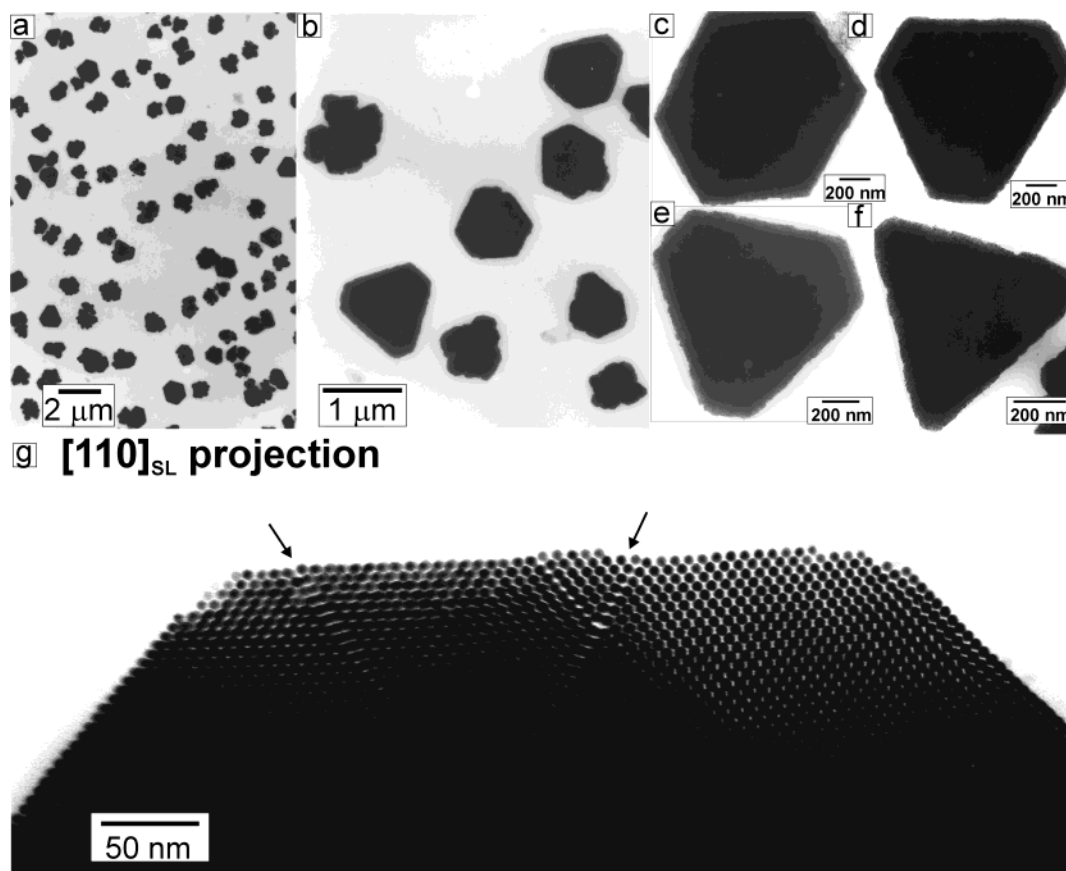
7444 *J. Phys. Chem. B, Vol. 107, No. 30, 2003*

Stoeva et al.

Figure 5. TEM micrographs of nanocrystal superlattices of Au nanoparticles prepared by the inverse micelle method: (a) and (b) low-magnification images; (c)−(f) regularly shaped nanocrystal superlattices; (g) magnified image of a superlattice edge (note the perfect arrangement of the Au nanoparticles).

tices evenly distributed on the TEM support. Many of the 3D structures are well faceted, and regularly shaped superlattices (Figure 5c−f) are abundant in the samples. Nearly perfect hexagonal and truncated hexagonal nanocrystal superlattices are illustrated in Figure 5c−f. These results were repeatedly obtained. It is reasonable to consider that the NCSLs presented in Figure 5 are equilibrium structures, and that no kinetic factors (such as solvent evaporation rate, film drying, etc.) are involved in the growth process. There are several facts which support this statement. Previously we demonstrated that dodecanethiol-stabilized gold colloidal solutions prepared by the inverse micelle method have reversible temperature-dependent solubility.[14,42] At room temperature such colloids precipitate and the sediment is composed of nanocrystal superlattices like those shown in Figure 5. Upon heating the superlattice structures dissolve back to separate nanoparticles in a fashion similar to molecular crystals. Deposition of a hot colloidal solution on a support leads to NCSLs despite the faster solvent evaporation. These facts indicate that superlattices can directly form in the colloidal solution (not only on a support), meaning that they are equilibrium structures. Nanocrystal superlattice growth was also tested on different chemically modified supports. TEM, AFM, and XRD did not show any difference between the superlattices (crystal structure, superlattice parameter) despite the different wetting behavior and drying rates on the various substrates.[43] All these results suggest that the NCSLs formed by gold nanoparticles prepared by the inverse micelle method are equilibrium structures.

Figure 5g represents a magnified image of a superlattice edge. This nanocrystal superlattice is remarkable in the perfect arrangement of practically monodisperse Au nanoparticles. The
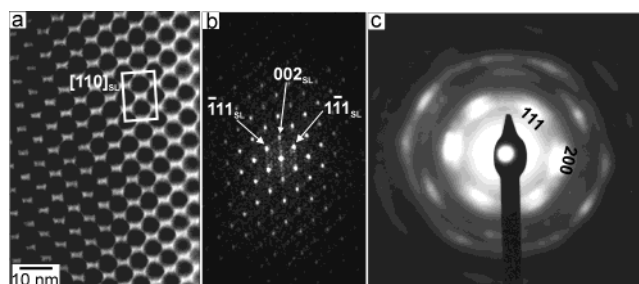

Figure 6. (a) TEM image of $[110]_{SL}$ projection of the Au nanocrystal superlattice shown in Figure 5g. The projected unit cell is represented by a rectangle. (b) and (c) are the corresponding small-angle and wide-angle electron diffraction patterns, respectively.

packing structure is fcc imaged in $[110]_{SL}$ projection (the subscript "SL" designates planes and directions in the nanocrystal superlattice). Unambiguous evidence for the fcc packing is the $[110]_{SL}$ small-angle electron diffraction pattern in Figure 6b. The high order present in the small-angle diffraction pattern confirms the existence of very long-range translational ordering of the Au nanoparticles in the superlattice structure. Figure 6a is a magnified region of the superlattice shown in Figure 5g. The $[110]_{SL}$ projected unit cell is represented by a rectangle. The superlattice parameter a was measured numerous times with many samples, and a was usually 8.9−9.2 nm, with occasional values as high as 11.0 nm. The {111} and {200} atomic lattice spacings in separate Au nanoparticles present in the same photograph as the superlattice of interest were used as an absolute calibration for determining the superlattice constant. The arrangement in the superlattice presented in Figure 5g is perfect to the extent that dislocations cause extended packing
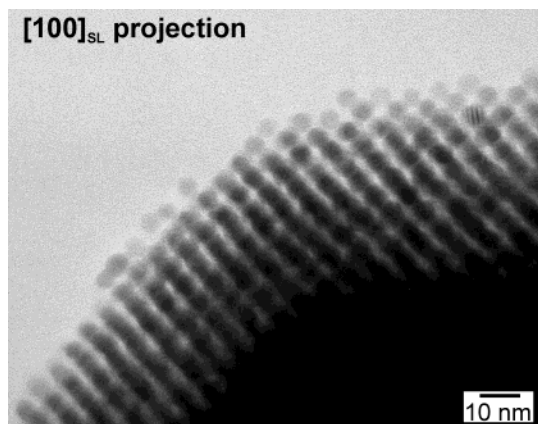
fcc and hcp Superlattices of Au Nanoparticles

J. Phys. Chem. B, Vol. 107, No. 30, 2003 **7445**

Figure 7. TEM micrograph of a nanocrystal superlattice composed of Au nanoparticles obtained by the inverse micelle method viewed along the $\langle 100 \rangle_{SL}$ direction.

defects to be developed (a typical phenomenon for natural crystals). The two dislocation shifts (indicated by arrows in Figure 5g) follow the $\langle 112 \rangle$ direction of the fcc lattice and correspond to a partial dislocation with a Burger vector $1/6\langle 112 \rangle$. This dislocation causes disordering of the ABCABCABC... type of packing with the formation of an ABC**ABA**BCABC... defect.

The wide-angle electron diffraction illustrated in Figure 6c shows discrete reflections indicative of the presence of an average coherent particle−particle alignment of the atomic lattice planes of the separate nanocrystals comprising the superlattice. Such orientational ordering is indicative of the faceted morphology of the Au nanoparticles and their inherent anisotropy. This finding is important since many optical and electronic properties of the nanocrystal assemblies will depend on the orientation of the building nanocrystals. Nanocrystal superlattices with orientational ordering were previously observed from metal[15,44] and semiconductor nanoparticles.[3]

The most frequently encountered alignment of the Au nanocrystal superlattices on the TEM support was along the $\langle 110 \rangle_{SL}$ direction. In some cases $[100]_{SL}$ orientation was observed (Figure 7). Figure 8a,b illustrates tapping-mode AFM images of $[100]_{SL}$ surfaces of gold nanocrystal superlattices formed on carbon-coated glass slides. The superlattice parameter a found by AFM is 8.2 ± 0.4 nm. This result is in agreement with the fcc superlattice constant determined by electron microscopy. Well-resolved Au nanoparticles with sizes between 4.5 and 5 nm are visible from the images. It should be pointed

out that we have not observed the artificial widening of the nanoparticle lateral size due to the convolution of the tip apex with the sample.[45] This is related to the close arrangement of the particles in the superlattice. Thus, the tip maps only the top part of the particles obviating the main cause of the enlargement phenomenon, namely tapping on the sides of the particles.[46]

X-ray diffraction was used to probe statistically large areas of nanocrystal superlattices grown on different substrates. Here, we present an XRD pattern (Figure 9) of gold colloidal crystals formed as a thin film on a carbon-coated glass slide (the same sample shown in Figure 4). The XRD contains many strong and sharp equally spaced reflections at 2θ angles lower than those corresponding to diffraction by gold atomic lattice planes. This is indicative of the presence of a large unit cell due to superlattice formation. The reflections in the XRD pattern can be indexed as $\{hhh\}_{SL}$ of a fcc structure with a unit cell constant of 8.9 nm. Such an assignment is in good agreement with the superlattice parameter determined by TEM and AFM. X-ray diffraction is particularly sensitive to periodicity perpendicular to the support.[8] The fact that all peaks in the diffraction pattern belong to one group of planes ($\{hhh\}_{SL}$) indicates a preferential alignment of the colloidal crystals with $\{111\}_{SL}$ planes parallel to the support. Such orientation could be related to the faceted morphology of the gold nanoparticles participating in the superlattice.

The TEM micrograph presented in Figure 10 is another indication of the faceted morphology of the particles prepared by the inverse micelle method. The superlattice is imaged under defocus conditions, which in some cases allow observing the shape of the particles, as well as the distribution of the ligand molecules on the particle surface.[28] The TEM image shows a $[110]_{SL}$ superlattice projection, and the faceted morphology of the particles is visible. From the enlarged micrograph in Figure 10, one can see the thiol molecules protruding from the gold cores in discrete directions. Such a preferred orientation of the ligands could be related to the fact that they preferentially adsorb on different facets of the particle surface. A possible rationale for the preferential fcc packing in the inverse micelle case is the faceted morphology of the gold cores, which leads to the adsorption of the thiol molecules on selected facets of the particle surface. This in turn influences the packing of the particles in the most energetically favorable arrangement for both the gold cores and the adsorbed ligands leading to the formation of equilibrium structures such as those observed in Figures 4 and 5.
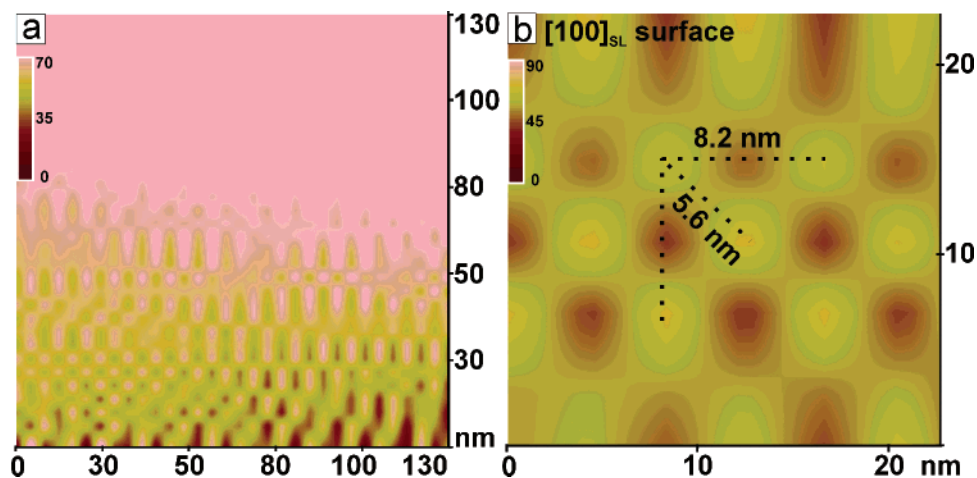

Figure 8. Tapping-mode AFM images of superlattices of Au nanoparticles synthesized by the inverse micelle method and deposited on carbon-coated glass slides. (a) Large area scan; (b) resolved $[100]_{SL}$ surface.

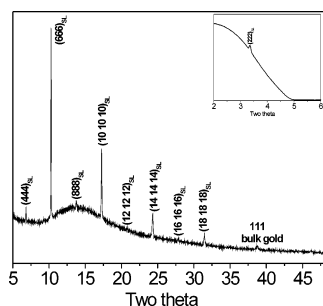**Figure 9.** XRD pattern of gold colloidal crystals (shown in Figure 4) grown on a carbon-coated glass slide (inverse micelle method).
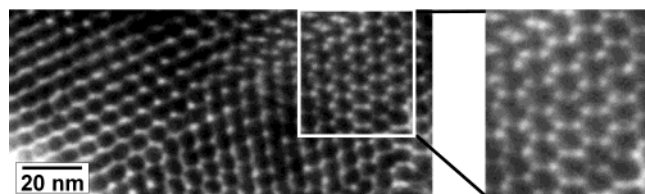

Figure 10. TEM micrograph of $[110]_{SL}$ superlattice (inverse micelle case). Note the faceted shape of the particles and the directionality of the ligands protruding from the particle surface (enlarged image).

Nanocrystal Superlattices of Au Nanoparticles Prepared by the SMAD Method.

The SMAD technique allows the reproducible preparation of large amounts of monodisperse Au colloidal solutions.[13] Dodecanethiol-stabilized Au particles prepared by this method have an average size of 4.5 nm [13] and a strong propensity toward superlattice formation when deposited on a support. Low-magnification TEM (Figure 11a) reveals large areas of nanocrystal superlattices evenly spread on the substrate. One of the structures laterally extends over a region of ~20 μm. Magnified images of the nanocrystal assemblies are presented in Figure 11b,c. A closer look at Figure 11b reveals a triangular particle pattern (see the inset). Such a triangular shape contrast is only typical for an hcp ordering as theoretically proven by Bentzon and Tholen.[47] Similar patterns were observed by Whetten and co-workers in hcp superlattices of Ag nanoparticles.[16] The hcp packing in our case is further supported by the small-angle electron diffraction pattern (Figure 12b) showing a well-defined 6-fold projected symmetry along the [0001] direction. The presence of a third order in the diffraction pattern agrees with the perfect translational ordering of the Au nanoparticles in the lattice. Figure 11c illustrates a flawless hcp nanocrystal superlattice oriented along the [0001] direction. The hcp superlattice constant *a* was found to be 8 ± 0.2 nm. A magnified $[0001]_{SL}$ projected TEM image of a nanocrystal superlattice and the corresponding schematic representation of hcp ordering viewed along $[0001]_{SL}$ are shown in parts a and b, respectively, of Figure 12. One can clearly see the contrast sequence in the particle packing.

The Au nanoparticles prepared by the SMAD method have predominantly spherical shapes as discussed earlier. The stabilizing molecules are anticipated to adsorb more evenly on the particle surface. Compared to the particles prepared by the inverse micelle method, no directional ordering of the ligand molecules would be expected for the SMAD nanoparticles. Such particles behave like "hard" spheres, and the most likely way of "hard" sphere arrangement is the hcp fashion.[16] The lack of directional interaction causes the nanoparticles to stick on random sites of the growing hcp lattice, which in turn leads to the absence of well-defined overall shapes of the superlattice crystal. It is important to note that this method of growth does
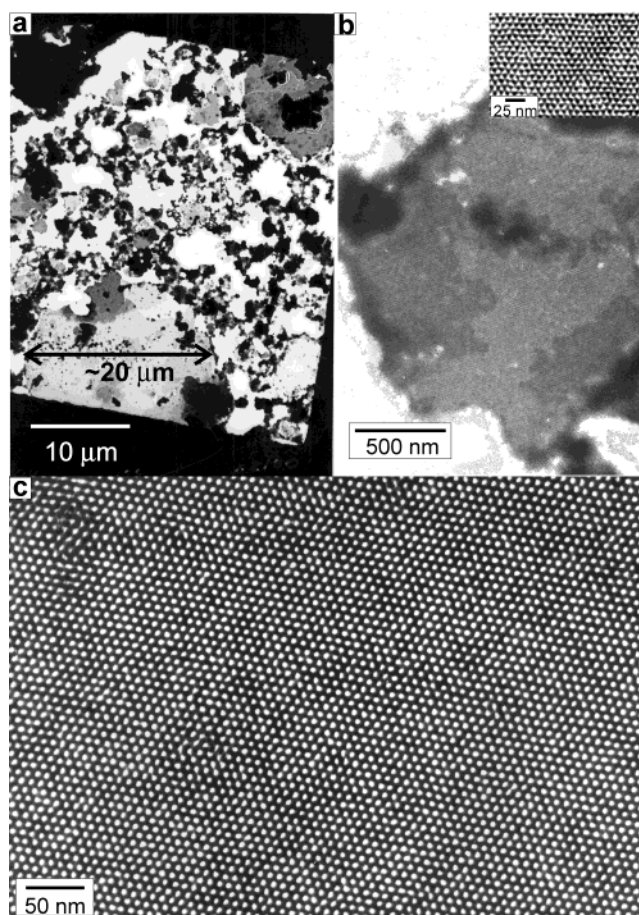

Figure 11. TEM micrographs of hcp nanocrystal superlattices of Au nanoparticles prepared by the SMAD method. (a) Low-magnification image; (b) and (c) magnified images. The inset in (b) demonstrates the triangular shape contrast typical for hcp ordering. Note the perfect particle arrangement in (c).

not influence the quality of the lattice itself as is visible from Figure 11c. Most probably, superlattice formation in the case of the SMAD nanoparticles takes place only on a support surface but not in solution. We want to point out that TEM of the nanocrystal superlattices reproducibly showed hcp structures as those illustrated and discussed in Figures 11 and 12. The lack of faceting and the presence of multiple defects in the core particle structure lead to a lack of orientational ordering in the superlattices. The wide-angle electron diffraction of the superlattice (Figure 12d) is an indication of this. The ring diffraction pattern suggests no coherent alignment of the atomic lattice planes in neighboring particles. Such behavior is a direct consequence of the defect nature of the gold cores constructing the superlattices. Despite the lack of orientational ordering, nanocrystal superlattices grown from Au particles prepared by the SMAD method have a perfect translational ordering. With this example, we prove again that the nanoparticle core morphology plays an important role in determining the superlattice structure.

AFM study of the surface ordering in nanocrystal superlattices of Au nanoparticles obtained by the SMAD method shows resolved $[100]_{SL}$ surfaces of an fcc superlattice with a lattice constant *a* of 8 ± 0.4 nm (Figure 13). This result does not agree with the TEM investigation, which showed hcp type of ordering. One possible reason might be a reconstruction taking place at the superlattice surface. AFM maps only the surface layer, which can be strongly influenced by different surface phenomena (surface tension, interaction with the surrounding liquid during
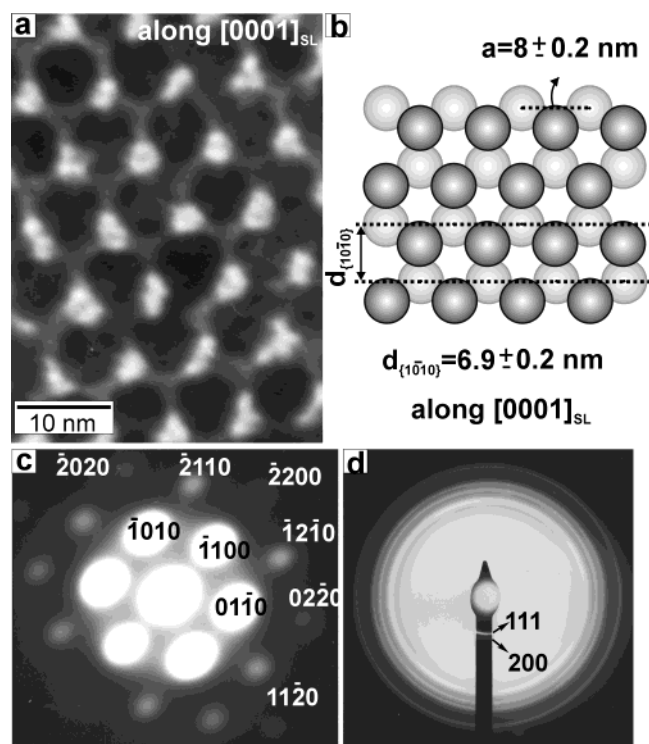
fcc and hcp Superlattices of Au Nanoparticles

J. Phys. Chem. B, Vol. 107, No. 30, 2003 **7447**

Figure 12. (a) High-magnification TEM micrograph of hcp ordered superlattice formed by Au particles prepared by the SMAD method (note the particle contrast). (b) Schematic representation of the hcp ordering viewed along [0001]$_{SL}$; (c) and (d) are the corresponding small-angle and wide-angle electron diffraction patterns.
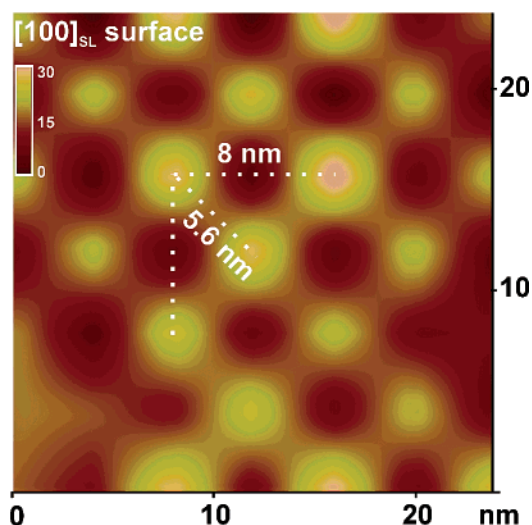

Figure 13. Tapping-mode AFM image of a superlattice surface of Au nanoparticles synthesized by the SMAD method.

the drying process). Another explanation could be related to the rates at which the superlattice crystals grow on the supports for TEM, AFM, and XRD. Samples for AFM and XRD are prepared over a much longer period of time compared to the TEM samples (see Experimental Section). The reason for this is the overall larger amount of sample deposited on the support in the case of AFM and XRD compared to TEM preparation. It is feasible to expect that both hcp and fcc superlattice structures can be formed in the case of Au nanoparticles synthesized by the SMAD method depending upon the solvent evaporation rate. This could be expected due to the following considerations. Several calculations have demonstrated that the free energies per particle of hcp and fcc hard-sphere crystals

(note that SMAD Au nanoparticles behave as hard spheres) are the same within the uncertainty of no more than $\sim 2 \times 10^{-3} k_{B}T$.[48,49] Molecular dynamic simulations of hard sphere packing have shown that a series of structures with packing fractions between 0.74 (fcc structure) and 0.64 (random close packed state) can be formed depending upon the compression rate used in the simulation.[50] The compression rate can be directly correlated to the drying rate in the case of superlattice formation. The study predicts that the final packing fraction can be statistically controlled by the compression rate.[50] There is a correlation between structure and the rate at which crystals composed of hard spheres grow.[48] Crystals grown slowly show a tendency toward fcc packing.[48] Thus it is likely that in the case of samples prepared for AFM and XRD (large amount of colloid, slower overall evaporation) both fcc and hcp structures can be formed by SMAD nanoparticles. The very fast evaporation of the colloid for TEM is likely to favor hcp ordering. XRD is needed in order to get information about statistically large areas of the samples. All gold superlattices of nanoparticles prepared by the SMAD method grown as thin films on a substrate give very strong XRD reflections. Currently, we cannot unambiguously index the XRD pattern to either hcp or fcc structures. Efforts are currently ongoing with synchrotron small-angle XRD to elucidate this problem.

Conclusions

The present paper demonstrates that dodecanethiol-stabilized Au nanoparticles prepared by two different synthetic routes preferentially organize into nanocrystal superlattices with different packing structures despite similarity in nanoparticle average size. Au nanocrystals synthesized by gold salt reduction in an inverse micelle system have predominantly faceted defect-free core morphologies and preferentially organize into fcc structures under equilibrium control with both translational and particle–particle orientational ordering proven by TEM, SAED, AFM, and XRD. Au nanoparticles obtained by bulk gold vaporization (SMAD procedure) have primarily defective core structures, lack faceting, and behave like "hard" spheres. They prefer to organize into hcp-type superlattices with long-range translational ordering illustrated by TEM and SAED. We believe that the main reason for different packing behavior of the particles prepared by the two methods is due to differences in their core morphologies resulting from the different inherent nature of the synthetic processes used. Also, the SMAD particles seem to be more influenced by kinetic growth features as the superlattices form.

References and Notes

(1) Pileni, M. P. *J. Phys. Chem. B* **2001**, *105*, 3358−3371.

(2) Murray, C. B.; Kagan, C. R.; Bawendi, M. G. *Annu. Rev. Mater. Sci.* **2000**, *30*, 545−610.

(3) Collier, C. P.; Vossmeyer, T.; Heath, J. R. *Annu. Rev. Phys. Chem.* **1998**, *49*, 371−404.

(4) Mirkin, C. A.; Letsinger, R. L.; Mucic, R. C.; Storhoff, J. J. *Nature* **1996**, *382*, 607−609.

(5) Alivisatos, A. P.; Johnson, K. P.; Peng, X.; Wilson, T. E.; Loweth, C. J.; Bruchez, M. P.; Schultz, P. G. *Nature* **1996**, *382*, 609−611.

(6) Collier, C. P.; Saykally, R. J.; Shiang, J. J.; Henrichs, S. E.; Heath, J. R. *Science* **1997**, *277*, 1978.

(7) Andres, R. P.; Bielefeld, J. D.; Henderson, J. I.; Janes; D. B.; Kolagunta, V. R.; Kubiak, C. P.; Mahoney, W. J.; Osifchin, R. *Science* **1996**, *273*, 1690−1693.

(8) Murray, C. B.; Kagan, C. R.; Bawendi, M. G. *Science* **1995**, *270*, 1335−1338.

(9) Heath, J. R.; Knobler, C. M.; Leff, D. V. *J. Phys. Chem. B* **1997**, *101*, 189−197.

(10) Whetten, R. L.; Khoury, J. T.; Alvarez, M. M.; Murthy, S.; Vezmar, I.; Wang, Z. L.; Stephens, P. W.; Cleveland, W. D.; Luedtke, W. D.; Landman, U. *Adv. Mater.* **1996**, *8*, 428−433.

(11) Lin, X. M.; Wang, G. M.; Sorensen, C. M.; Klabunde, K. J. *J. Phys. Chem. B* **1999**, *103*, 5488−5492.

(12) Lin, X. M.; Jaeger, H. M.; Sorensen, C. M.; Klabunde, K. J. *J. Phys. Chem. B* **2001**, *105*, 3353−3357.

(13) Stoeva, S.; Klabunde, K. J.; Sorensen, C. M.; Dragieva, I. *J. Am. Chem. Soc.* **2002**, *124*, 2305−2311.

(14) Prasad, B. L. V.; Stoeva, S. I.; Sorensen, C. M.; Klabunde, K. J. *Langmuir* **2002**, *18*, 7515−7520.

(15) Harfenist, S. A.; Wang, Z. L.; Alvarez, M. M.; Vezmar, I.; Whetten, R. L. *J. Phys. Chem. B* **1996**, *100*, 13904−13910.

(16) Harfenist, S. A.; Wang, Z. L.; Whetten, R. L.; Vezmar, I.; Alvarez, M. M. *Adv. Mater.* **1997**, *9*, 817−822.

(17) Wang, Z. L.; Harfenist, S. A.; Vezmar, I.; Whetten, R. L.; Bentley, J.; Evans, N. D.; Alexander, K. B. *Adv. Mater.* **1998**, *10*, 808−812.

(18) Keely, C. J.; Fink, J.; Brust, M.; Bethell, D.; Schiffrin, D. J. *Nature* **1998**, *396*, 444.

(19) Martin, J. E.; Wilcoxon, J. P.; Odinek, J.; Provencio, P. *J. Phys. Chem. B* **2000**, *104*, 9475−9486.

(20) Martin, J. E.; Wilcoxon, J. P.; Odinek, J.; Provencio, P. *J. Phys. Chem. B* **2002**, *106*, 971−978.

(21) Murray, C. B.; Sun, S.; Gaschler, W.; Doyle, H.; Betley, T. A.; Kagan, C. R. *IBM J. Res. Dev.* **2001**, *45*, 47−56.

(22) Alivisatos, A. P. *Science* **1996**, *271*, 933−937.

(23) Pinna, N.; Weiss, K.; Sack-Kongehl, H.; Vogel, W.; Urban, J.; Pileni, M. P. *Langmuir* **2001**, *17*, 7982−7987.

(24) Sun, S.; Murray, C. B. *J. Appl. Phys.* **1999**, *85*, 4325−4330.

(25) Sun, S.; Murray, C. B.; Weller, D.; Folks, L.; Moser, A. *Science* **2000**, *287*, 1989−1992.

(26) Petit, C.; Taleb, A.; Pileni, M. P. *J. Phys. Chem. B* **1999**, *103*, 1805−1810.

(27) Shevchenko, E. V.; Talapin, D. V.; Rogach, A. L.; Kornowski, A.; Haase, M.; Weller, H. *J. Am. Chem. Soc.* **2002**, *124*, 11480−11485.

(28) Wang, Z. L. *Adv. Mater.* **1998**, *10*, 13−30.

(29) Zanchet, D.; Moreno, M. S.; Ugarte, D. *Phys. Rev. Lett.* **1999**, *82*, 5277−5280.

(30) Wang, Z. L.; Harfenist, S. A.; Whetten, R. L.; Bentley, J.; Evans, N. D. *J. Phys. Chem. B* **1998**, *102*, 3068−3072.

(31) Luedtke, W. D.; Landman, U. *J. Phys. Chem. B* **1996**, *100*, 13323−13329.

(32) Whetten, R. L.; Shafigullin, M. N.; Khoury, J. T.; Schaaff. T. G.; Vezmar, I.; Alvarez, M. M.; Wilkinson, A. *Adv. Mater.* **1999**, *32*, 397−406.

(33) Gutierrez, C.; Santiago, P.; Ascencio, J. A.; Camacho, A.; Jose-Yacaman, M. *Appl. Phys. A* **2000**, *71*, 237−243.

(34) Korgel, B. A.; Fitzmaurice, D. *Phys. Rev. B* **1999**, *59*, 14191−14201.

(35) Klabunde, K. J.; Timms, P. L.; Skell, P. S.; Ittel, S. *Inorg. Synth.* **1979**, *19*, 59−86.

(36) Doraiswamy, N.; Marks, L. D. *Philos. Mag. B* **1995**, *71*, 291−310.

(37) Marks, L. D. *Rep. Prog. Phys.* **1994**, *57*, 603−649.

(38) Zanchet, D.; Hall, B. D.; Udarte, D. *J. Phys. Chem. B* **2000**, *104*, 11013−11018.

(39) Ino, S. *Phys. Soc. Jpn.* **1966**, *21*, 346.

(40) Stoeva, S. I.; et al. Unpublished results from this laboratory.

(41) Burton, W. K.; Cabrera, N.; Frank, F. C. *Philos. Trans. R. Soc. London, Ser. A* **1951**, *243*, 299−358.

(42) Lin, X. M.; Sorensen, C. M.; Klabunde, K. J. *Chem. Mater.* **1999**, *11*, 198−202.

(43) Stoeva, S. I.; et al. Unpublished results from this laboratory.

(44) Brown, L. O.; Hutchinson, J. E. *J. Phys. Chem. B* **2001**, *105*, 8911−8916.

(45) Ramirez-Aguilar, K. A.; Rowlen, K. L. *Langmuir* **1998**, *14*, 2562−2566.

(46) Maeda, H.; Maeda, Y. *Nano Lett.* **2002**, *2*, 1073−1077.

(47) Bentzon, M. D.; Tholen, A. R. *Ultramicroscopy* **1991**, *38*, 105−115.

(48) Pusey, P. N.; Megen, W.; Bartlett, P.; Ackerson, B. J.; Rarity, J. G.; Underwood, S. M. *Phys. Rev. Lett.* **1989**, *63*, 2753−2756.

(49) Igloi, F. *J. Phys. C* **1986**, *19*, 6907−6914.

(50) Truskett, T. M.; Torquato, S.; Debenedetti, P. G. *Phys. Rev. E* **2000**, *62*, 993−1001.